Check for updates

SFPQ-ABL1 and BCR-ABL1 use different signaling networks to drive B-cell acute lymphoblastic leukemia

Lauren M. Brown,[1-5] Soroor Hediyeh-zadeh,[6,7] Teresa Sadras,[8,9] Hannah Huckstep,[6] Jarrod J. Sandow,[6,7] Ray C. Bartolo,[4] Hansen J. Kosasih,[4] Nadia M. Davidson,[4,8,10] Breon Schmidt,[4,8] Stefan Bjelosevic,[8,9] Ricky Johnstone,[8,9] Andrew I. Webb,[6,7] Seong L. Khaw,[4,6,11] Alicia Oshlack,[4,8,10] Melissa J. Davis,[6,7,12,*] and Paul G. Ekert[1-5,8,*]

[1]Children's Cancer Institute, Lowy Cancer Research Centre, UNSW Sydney, Sydney, NSW, Australia; [2]School of Women's and Children's Health, UNSW Sydney, Sydney, NSW, Australia; [3]University of New South Wales Centre for Childhood Cancer Research, UNSW Sydney, Sydney, NSW, Australia; [4]Murdoch Children's Research Institute, Parkville, VIC, Australia; [5]Department of Paediatrics, University of Melbourne, Parkville, VIC, Australia; [6]Walter and Eliza Hall Institute of Medical Research, Parkville, VIC, Australia; [7]Department of Medical Biology, Faculty of Medicine, Dentistry and Health Sciences, The University of Melbourne, Melbourne, VIC, Australia; [8]Peter MacCallum Cancer Centre, Parkville, VIC, Australia; [9]The Sir Peter MacCallum Department of Oncology, University of Melbourne, Parkville, VIC, Australia; [10]School of BioSciences, University of Melbourne, Parkville, VIC, Australia; [11]Royal Children's Hospital, Parkville, VIC, Australia; and [12]Department of Clinical Pathology, Faculty of Medicine, Dentistry and Health Sciences, The University of Melbourne, Melbourne, VIC, Australia

Key Points

- SFPQ-ABL1 is localized to the nuclear compartment and is a relatively weaker driver of cellular proliferation compared with BCR-ABL1.

- SFPQ-ABL1 and BCR-ABL1 activate distinct signaling networks, both of which converge on inhibiting apoptosis and driving proliferation.

Philadelphia-like (Ph-like) acute lymphoblastic leukemia (ALL) is a high-risk subtype of B-cell ALL characterized by a gene expression profile resembling Philadelphia chromosome–positive ALL (Ph[+] ALL) in the absence of *BCR-ABL1*. Tyrosine kinase–activating fusions, some involving *ABL1*, are recurrent drivers of Ph-like ALL and are targetable with tyrosine kinase inhibitors (TKIs). We identified a rare instance of *SFPQ-ABL1* in a child with Ph-like ALL. *SFPQ-ABL1* expressed in cytokine-dependent cell lines was sufficient to transform cells and these cells were sensitive to ABL1-targeting TKIs. In contrast to BCR-ABL1, SFPQ-ABL1 localized to the nuclear compartment and was a weaker driver of cellular proliferation. Phosphoproteomics analysis showed upregulation of cell cycle, DNA replication, and spliceosome pathways, and downregulation of signal transduction pathways, including ErbB, NF-κB, vascular endothelial growth factor (VEGF), and MAPK signaling in *SFPQ-ABL1*–expressing cells compared with *BCR-ABL1*–expressing cells. SFPQ-ABL1 expression did not activate phosphatidylinositol 3-kinase/protein kinase B (PI3K/AKT) signaling and was associated with phosphorylation of G2/M cell cycle proteins. SFPQ-ABL1 was sensitive to navitoclax and S-63845 and promotes cell survival by maintaining expression of Mcl-1 and Bcl-xL. SFPQ-ABL1 has functionally distinct mechanisms by which it drives ALL, including subcellular localization, proliferative capacity, and activation of cellular pathways. These findings highlight the role that fusion partners have in mediating the function of ABL1 fusions.

Introduction

Philadelphia-like (Ph-like) ALL is a high-risk subtype of B-cell acute lymphoblastic leukemia (B-ALL) associated with increased rates of relapse and poor clinical outcomes.[1] Ph-like ALL is characterized

by a gene expression signature akin to that of Philadelphia chromosome–positive (Ph+) ALL in the absence of the *BCR-ABL1* fusion gene.[2,3] Instead, Ph-like ALL cases commonly harbor other cytokine receptor and tyrosine kinase–activating lesions.[1] The clinical success of tyrosine kinase inhibitors (TKIs) in Ph+ ALL emphasize the importance of early identification of these potentially targetable lesions.[4-6] Patients with Ph-like ALL harboring *ABL*-class rearrangements (*ABL1*, *ABL2*, *CSF1R*, or *PDGFRB*) exhibited improved outcomes when treated with TKIs at diagnosis or relapse.[7] However, some ABL1 fusion proteins may be less sensitive to ABL1 inhibitors. For example, SNX2-ABL1 shows reduced sensitivity in vitro to multiple TKIs targeting ABL1[8] and is associated with poor clinical response to dasatinib.[9,10] Understanding the sensitivity of specific molecular aberrations in Ph-like ALL can inform the selection of the most appropriate treatments.

To date, 12 *ABL1* partner genes have been described in B-ALL: *BCR*, *CENPC*, *ETV6*, *FOXP1*, *LSM14A*, *NUP153*, *NUP214*, *RANBP2*, *RCSD1*, *SFPQ*, *SNX2*, and *ZM1Z1*.[1,9,11-13] Notably, 4 of these fusion genes, *FOXP1-ABL1*, *RCSD1-ABL1*, *SNX2-ABL1*, and *SFPQ-ABL1*, have a different *ABL1* breakpoint compared with *BCR-ABL1*.[9,14-16] These fusion partners link to exon 4 of *ABL1*, resulting in chimeric proteins lacking the SRC Homology 3 (SH3) and part of the SRC Homology 2 (SH2) domain, normally retained in BCR-ABL1. The SH2 and SH3 domains regulate ABL1 kinase activation.[17] How the absence of these domains influences transforming capacity has not been specifically studied for rare ABL1 fusions.[18] Evidence from the study of BCR-ABL1 oncoproteins[19-21] and NUP214-ABL1[22,23] suggests that in addition to providing oligomerization domains, the N-terminal fusion partner also mediates intermolecular interactions and determines the subcellular localization of the fusion.

This study reports an *SFPQ-ABL1* fusion identified in an 8-year-old patient with B-ALL.[24] *SFPQ-ABL1* is extremely rare, previously reported in 7 cases, with our case representing the youngest patient to date.[12,16,24-27] SFPQ is 1 of 3 proteins belonging to the Drosophila-Behavior, Human-Splicing (DBHS) family, also including NONO and PSPC1, which in part function in the formation of nuclear paraspeckles, RNA-protein bodies that mediate nuclear retention of messenger RNAs (mRNAs).[28-30] SFPQ is a multifunctional nuclear protein implicated in a range of additional cellular processes, including mRNA splicing, transcriptional regulation, translation, and 3′-end processing.[29,31-34] It is unknown whether SFPQ exerts its wild-type functions when fused to ABL1 or if *SFPQ-ABL1* expression alters wild-type SFPQ function.

Here we identify unique molecular features that distinguish SFPQ-ABL1 from BCR-ABL1. As with BCR-ABL1, SFPQ-ABL1 promotes cell survival and was sensitive to TKIs that targeted ABL1. Unlike BCR-ABL1, SFPQ-ABL1 was localized to the nuclear compartment, activated distinct signaling networks, and was a comparatively weak driver of cellular proliferation. This study highlights the functional importance of the N-terminal partners in ABL1 fusion proteins and the unique mechanisms by which they function.

Methods

Ethics statement

This study was approved by the Royal Children's Hospital Human Research Ethics Committee (HREC 34127). Patients/families provided informed written consent for samples to be banked and subsequently used for research purposes, including the sequencing studies we have used to identify this fusion. Ethics approval did not require a second consenting procedure.

Case description and *SFPQ-ABL1* identification

The patient presented as an 8-year-old female with a peripheral blood white cell count of 43.5×10^9 cells/L and the presence of central nervous system (CNS-3) disease. Conventional karyotype analysis was performed as part of the patient's standard-of-care diagnostic testing (Victorian Clinical Genetics Services, Parkville, VIC, Australia). The abnormal karyotype identified a t(1;9)(p34;q34) chromosomal translocation, predicted to result in the *SFPQ-ABL1* gene fusion.[16] The presence of this rearrangement was also indicated by an abnormal interphase fluorescence in situ hybridization result using the standard *BCR/ABL1* Dual Color probe, showing diminished *ABL1* signal and gene splitting suggesting a t(1;9) translocation. The patient was treated on Children's Oncology Group AALL1131 induction protocol followed by Children's Oncology Group AALL1122, standard chemotherapy with dasatinib, and remained in remission at last follow-up, 4.5 years' post-diagnosis. The *SFPQ-ABL1* fusion transcript and specific breakpoint were retrospectively identified as part of a previously published ALL cohort,[24] using RNA sequencing (RNA-seq). RNA-seq and fusion detection were performed as previously described. The *SFPQ-ABL1* breakpoint and full-length fusion were polymerase chain reaction amplified from patient complementary DNA using previously published[16] and custom primers, respectively, and sequences were confirmed by Sanger sequencing (Australian Genome Research Facility, Melbourne, VIC, Australia). Visualization of fusion transcripts was produced by using Arriba,[35] and protein schematics were produced by using ProteinPaint.[36]

Functional studies

Detailed information on DNA constructs, cell culture, western blotting, viability and proliferation assays, drug treatment assays, and data analysis is provided in the supplemental Methods.

Immunofluorescence

Ba/F3 and primary pre–B cells expressing *BCR-ABL1*, *SFPQ-ABL1*, or murine stem cell virus (MSCV, empty vector control) were seeded in Nunc Laboratory-TekII chambers, fixed with 4% paraformaldehyde, permeabilized with methanol (Perm Buffer III; BD Biosciences, Franklin Lakes, NJ), and incubated overnight at 4°C with an anti-Abl antibody (Cell Signaling Technology, Danvers, MA). Anti-rabbit IgG AF-647 was used as a secondary antibody (Thermo Fisher Scientific, Waltham, MA). Cells were mounted with Prolong Gold anti-fade mounting media with 4′,6-diamidino-2-phenylindole (Thermo Fisher Scientific). Slides were viewed by using a Zeiss Elyra 780 confocal microscope (Zeiss, Oberkochen, Germany) and images analyzed with ZEN (black edition; Zeiss).

Phosphoproteomics sample preparation

Label-free quantification was performed on 4 biologically independent lines of MSCV, *BCR-ABL1*, *SFPQ-ABL1*, and *SFPQ-ABL1* + SH2/SH3 Ba/F3. MSCV Ba/F3 cells were maintained in RPMI 1640 (Sigma Aldrich, St. Louis, MO) supplemented with 10% fetal bovine serum (Thermo Fisher Scientific) and 0.5 ng/mL murine interleukin-3 (IL-3) (PeproTech, Cranbury, NJ), and all other cell lines
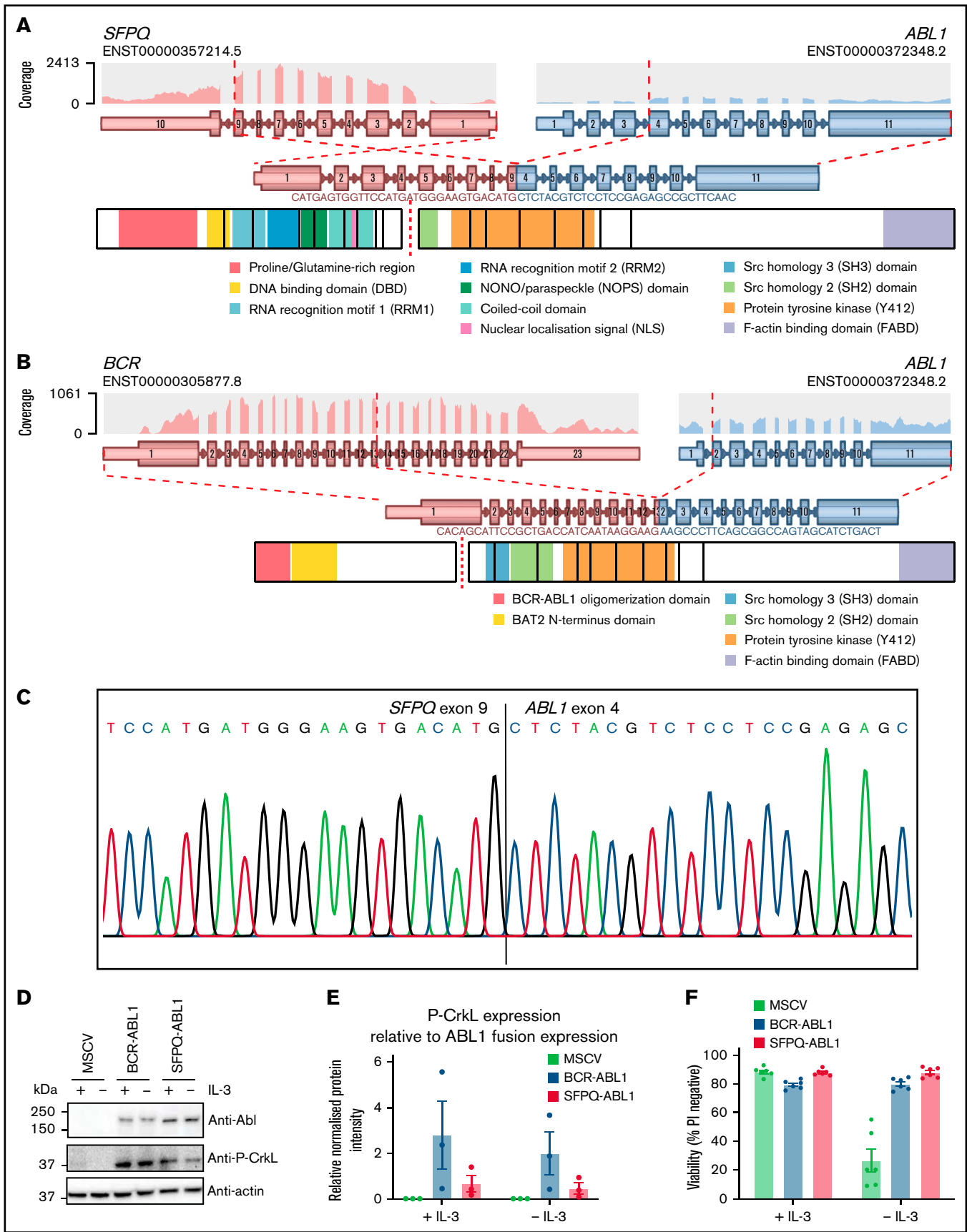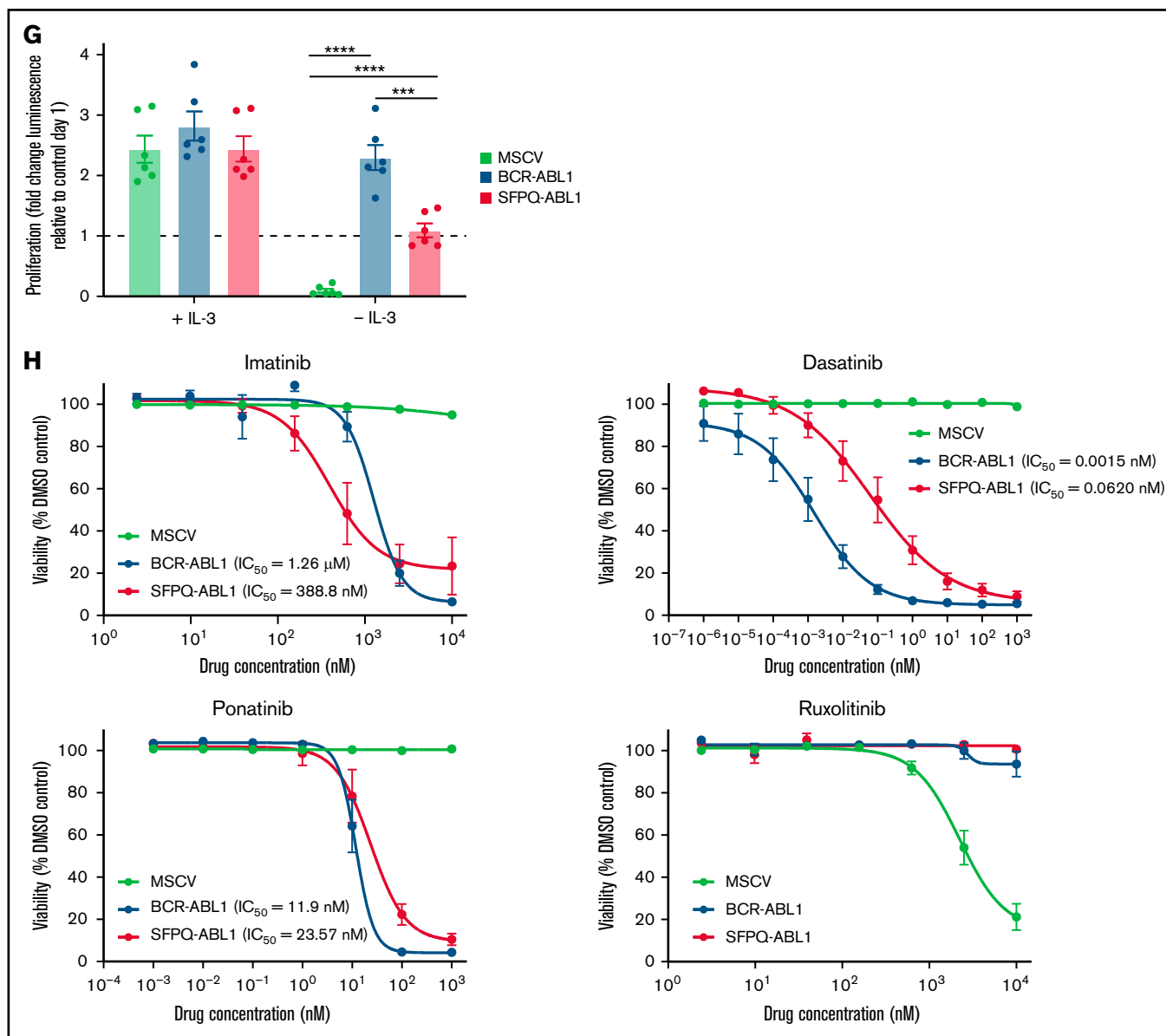
Figure 1.

Figure 1. SFPQ-ABL1 is sufficient to transform IL-3–dependent cell lines but is a relatively weaker driver of proliferation compared with BCR-ABL1. (A) Schematic of *SFPQ-ABL1* fusion transcript and resultant chimeric protein. (B) Schematic of *BCR-ABL1* fusion transcript, identified in a Ph+ patient from our RNA-seq cohort and resultant chimeric protein. (C) Sanger sequencing result of *SFPQ-ABL1* breakpoint polymerase chain reaction product amplified from patient complementary DNA, confirming fusion of exon 9 of *SFPQ* to exon 4 of *ABL1*. (D) western blot analysis of Abl and Phospho-CrkL (P-CrkL) (Y207) expression after 4-hour IL-3 withdrawal in *BCR-ABL1*– and *SFPQ-ABL1*–expressing Ba/F3 cells (representative western blot image is shown, n = 3). (E) Quantification of western blot analysis (shown in panel D) of P-CrkL expression relative to ABL1 fusion expression. Protein intensities were normalized to actin loading control. Data are presented as mean ± standard error of the mean (SEM) (n = 3). (F) Viability analysis of *BCR-ABL1*– and *SFPQ-ABL1*–expressing Ba/F3 cells after 48-hour IL-3 withdrawal. Viability was determined by propidium iodide (PI) exclusion, measured by flow cytometry. Data are presented as mean ± SEM (n = 6). (G) Proliferation of *BCR-ABL1*– and *SFPQ-ABL1*–expressing Ba/F3 cells after 48-hour IL-3 withdrawal. Proliferation was measured by luminescence relative to MSCV empty vector control at 24 hours (Day 1) using the CellTiter-Glo 2.0 reagent (Promega, Madison, WI). Groups were compared by using unpaired Student t tests with Holm-Šídák correction for multiple comparisons (error bars show mean ± SEM, n = 6). ***$P < .001$, ****$P < .0001$. (H) Viability analysis of *BCR-ABL1*– and *SFPQ-ABL1*–expressing Ba/F3 cells treated with a dose titration of imatinib, dasatinib, ponatinib, or ruxolitinib. Data are normalized to vehicle control (0.001% dimethyl sulfoxide [DMSO]; not shown on graphs) and nonlinear regression analysis was performed to fit dose–response curves. Data are presented as mean ± SEM (n = 3 for imatinib and ruxolitinib treatments, n = 8 for dasatinib and ponatinib).

were maintained in RPMI 1640 supplemented with 10% fetal bovine serum. Cell pellets were prepared for mass spectrometry. Complete details regarding sample preparation and mass spectrometry are provided in the supplemental Methods.

Raw mass spectrometer files were analyzed by using MaxQuant (version 1.5.8.3). The database search was performed by using the UniProt *Mus musculus* database (date of download, March 2018) plus common contaminants with strict trypsin specificity allowing up
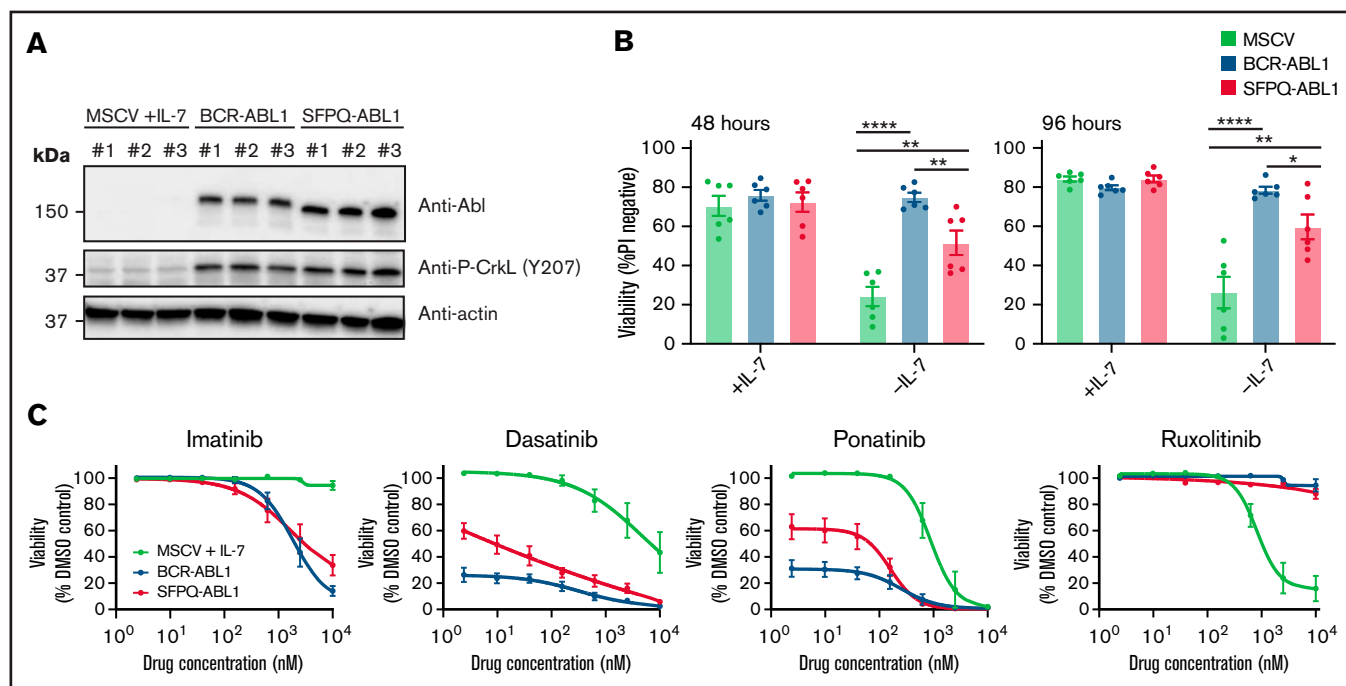
Figure 2. SFPQ-ABL1 transforms IL-7–dependent Pu.1/Irf4 DKO cells, and these cells are sensitive to TKIs that target ABL1. (A) western blot analysis of Abl and P-CrkL (Y207) expression in 3 biologically independent Pu.1/Irf4 DKO cell lines expressing *BCR-ABL1* or *SFPQ-ABL1*. (B) Viability analysis after 48- and 96-hour IL-7 withdrawal in Pu.1/Irf4 DKO cells expressing *BCR-ABL1* (blue) or *SFPQ-ABL1* (red). Viability was determined by propidium iodide (PI) exclusion, measured by flow cytometry. Groups were compared by using unpaired Student *t* tests with Holm-Šídák correction for multiple comparisons (error bars show mean ± standard error of the mean, n = 6). *$P < .05$, **$P < .01$, ****$P < .0001$. (C) Viability analysis of Pu.1/Irf4 DKO cells expressing MSCV, *BCR-ABL1*, or *SFPQ-ABL1* treated with a dose titration of imatinib, dasatinib, ponatinib, or ruxolitinib. Data are normalized to vehicle control (0.001% dimethyl sulfoxide [DMSO]; not shown on graphs), and nonlinear regression analysis was performed to fit dose–response curves. Data are presented as mean ± standard error of the mean (n = 3).

to 3 missed cleavages. Missing peptide expressions were imputed by using a method based on low-rank decomposition. The imputed data were corrected for technical variabilities inherent to proteomics experiments via Surrogate Variable Analysis implemented in R/Bioconductor package limma.[37] Tests for differential peptide expression (DPE) and differential peptide usage (DPU) were performed by using linear models with empirical Bayes moderated *t*-statistics using limma. The primary comparison performed in these analyses was *SFPQ-ABL1*–expressing cells vs *BCR-ABL1*–expressing cells; MSCV- and *SFPQ-ABL1*+SH2/SH3 mutant–expressing Ba/F3 cells were used as additional controls.

For peptides of interest, modified peptide sequences were aligned to *Mus musculus* protein sequences using the "search sequence" function of PhosphoSitePlus version 6.5.9.[38] Evidence of phosphorylation regulation annotated in PhosphoSitePlus was recorded for individual phosphorylation events.

Precursor ion intensities were quantified by MaxQuant in data-dependent acquisition mode. Fragment ion intensities in each sample were summarized at the modified peptide level by taking the median of values in that sample. Peptides with <4 observed values were discarded. Peptide intensities were log2-transformed and quantile normalized. Missing peptide intensities were imputed by fitting a rank 2 approximation model to the log-intensity data using msImpute.[39] Unwanted variations were estimated from imputed data using the wsva() function in limma,[37] and up to 5 surrogate variables were removed (regressed out) from the data. A linear model was fitted to each modified peptide, and statistical significance for differential

changes in fold-change (differential expression) between SFPQ-ABL1 and BCR-ABL1 was determined by empirical Bayes moderated *t*-statistic and 5% false discovery rate using limma.[40] For gene set enrichment analysis, peptide-level *P* values were converted to protein-level *P* values using Sime's test. The log fold change of each protein was determined as the log fold change of the peptide with the most significant *P* value. Enriched KEGG pathways were determined using protein-level statistics and kegga() function in limma. The differentially used peptides (peptides differentially phosphorylated relative to other peptides of the same protein) were identified by using diffSplice() and the *t*-test mode of topSplice() functions in limma.

Data-sharing statement

The mass spectrometry proteomics data have been deposited to the ProteomeXchange Consortium via the PRIDE[41] partner repository with the data set identifier PXD028925. Ba/F3 RNA-seq data are available the Gene Expression Omnibus database (accession number GSE185860). Patient RNA-seq data are available from the European Genome-Phenome Archive (accession number EGAS00001004212).

Results

SFPQ-ABL1 transforms cytokine-dependent cell lines but is a relatively weaker driver of proliferation compared with BCR-ABL1

We previously sequenced RNA from a cohort of pediatric patients with ALL as part of an RNA-seq utility study.[24] Analysis of RNA-seq
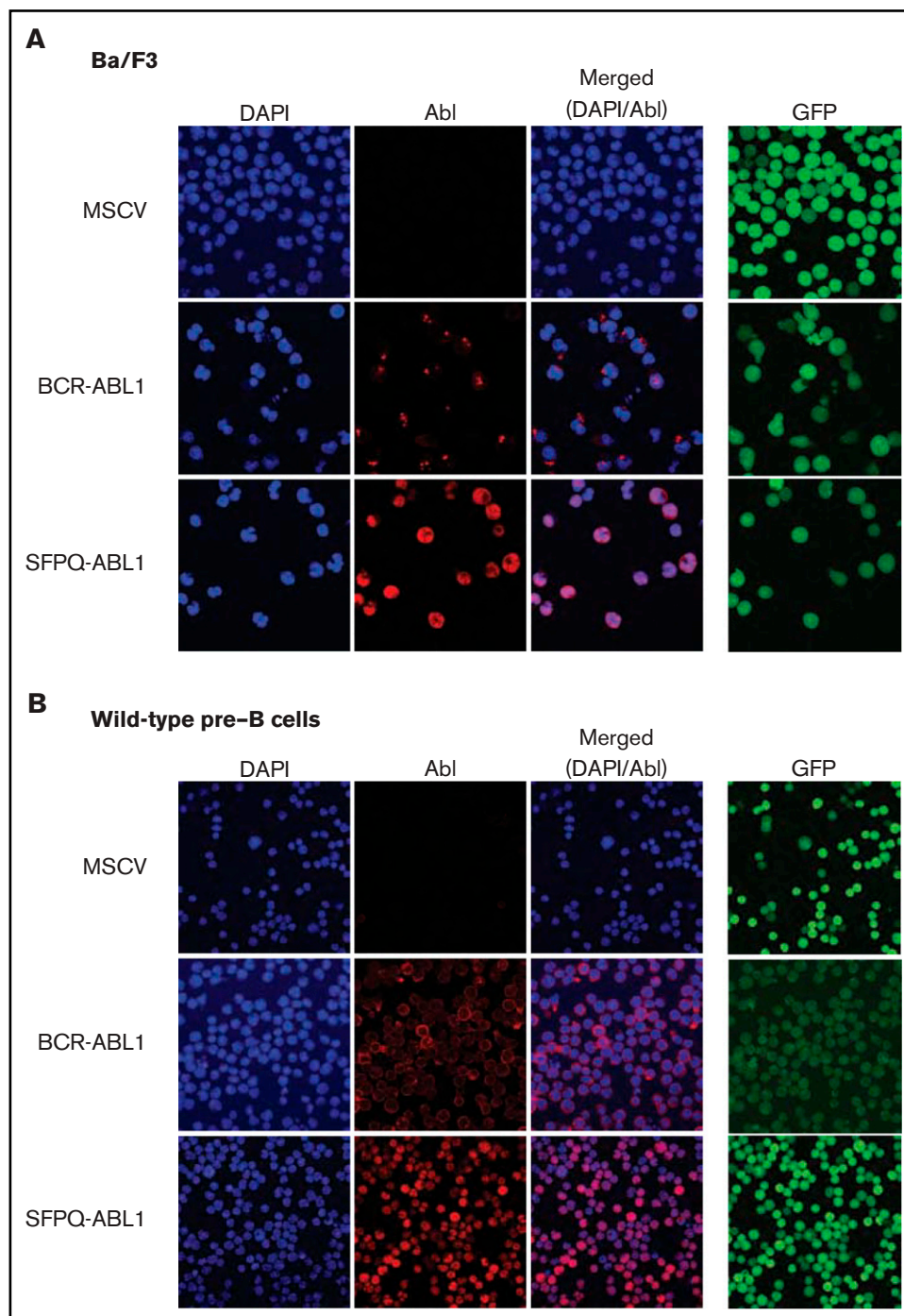
Figure 3. SFPQ-ABL1 localizes to the nucleus. Immunofluorescence analysis of Ba/F3 (A) and wild-type pre-B (B) MSCV (control), *BCR-ABL1*− or *SFPQ-ABL1*−expressing cells. Images were captured using ×40 magnification. Slides were viewed by using the Zeiss Elyra 780 confocal microscope and images analyzed using ZEN (black edition). DAPI, 4′,6-diamidino-2-phenylindole; GFP, green fluorescent protein.

data from 1 patient confirmed the presence of an *SFPQ-ABL1* fusion transcript, fusing exon 9 of *SFPQ* to exon 4 of *ABL1* (Figure 1A). This transcript lacks the SH3 domain and part of the SH2 domain, usually present in *BCR-ABL1* (Figure 1B). Given that the SH2 domain is known to facilitate interaction between BCR-ABL1 and signal transduction proteins, the absence of this domain in

SFPQ-ABL1 may contribute to differences in transformation and signaling. To confirm the transforming capacity of SFPQ-ABL1 and further explore functional and signaling differences compared with BCR-ABL1, the *SFPQ-ABL1* fusion transcript was amplified from patient complementary DNA and expressed in Ba/F3 cells (Figure 1C; supplemental Figure 1).
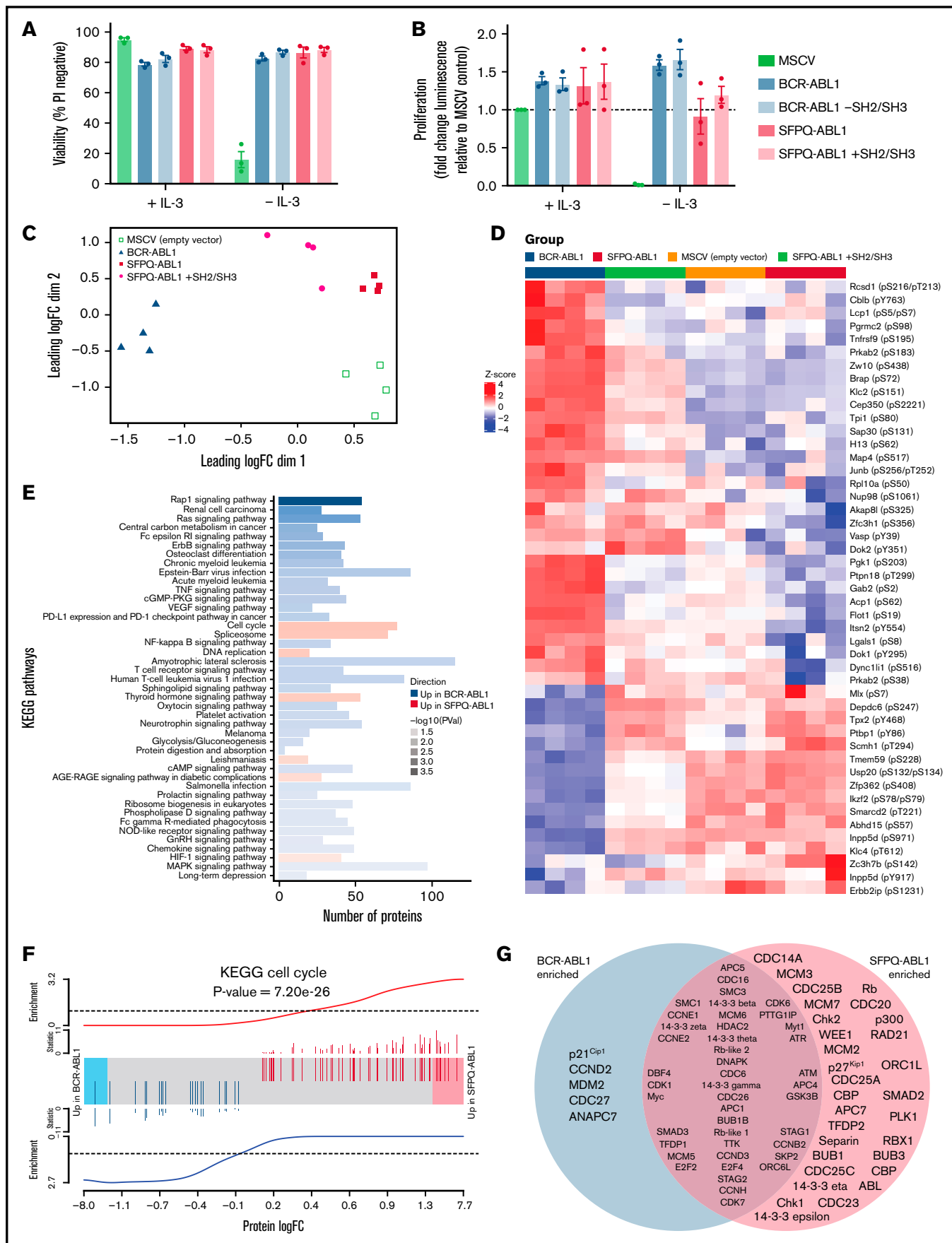
Figure 4.

The SFPQ-ABL1 fusion protein had a constitutively active ABL1 kinase domain, indicated by phosphorylation of a known ABL1[42] and BCR-ABL1[43] substrate, CrkL (Figure 1D). We showed that despite higher expression of the SFPQ-ABL1 fusion than the BCR-ABL1 fusion in Ba/F3 cells, BCR-ABL1 expression drives increased kinase activity, indicated by relatively increased levels of Phospho-CrkL (P-CrkL, Figure 1E; supplemental Figure 2). *SFPQ-ABL1* expression effectively blocked IL-3 withdrawal–induced cell death (Figure 1F) but was a weaker driver of IL-3–independent proliferation compared with BCR-ABL1 (Figure 1G; supplemental Figure 3). Importantly, Ba/F3 cells transformed by *SFPQ-ABL1* were sensitive to TKIs that target ABL1 but not the JAK inhibitor ruxolitinib (Figure 1H).

In addition to Ba/F3 cells, we expressed *SFPQ-ABL1* and *BCR-ABL1* in IL-7–dependent *Pu.1/Irf4* double knockout (DKO) pre–B cell lines (Figure 2A). This model mimics *Ikzf1* (encoding Ikaros) deletion, frequently observed in Ph+ and Ph-like ALL, as *Ikzf1* is a direct transcriptional target of Irf4 and Pu.1.[2,44,45] In this model, *BCR-ABL1* expression completely blocked IL-7 withdrawal–induced cell death (Figure 2B). Transformation by SFPQ-ABL1 was delayed, compared with BCR-ABL1 (supplemental Figure 4). To confirm this phenotype, we transduced IL-7–dependent wild-type pre–B cells, derived from wild-type C57BL/6 mice, with *BCR-ABL1* and *SFPQ-ABL1* and monitored cells by flow cytometry after IL-7 withdrawal. Here, we again observed delayed transformation by *SFPQ-ABL1*, compared with *BCR-ABL1* (supplemental Figure 5). Lastly, we showed that *SFPQ-ABL1*–expressing Pu.1/Irf4 DKO cells were sensitive to TKIs that target ABL1 (Figure 2C; supplemental Figure 6). Together, these data confirm that the SFPQ-ABL1 fusion is transforming and sensitive to ABL1-targeting TKIs but is a relatively weaker driver of cytokine-independent proliferation compared with BCR-ABL1.

SFPQ-ABL1 localizes to the nucleus

Given that wild-type SFPQ localizes to nuclear paraspeckles and the nucleosome, we speculated that SFPQ-ABL1, which retains one nuclear localization signal of SFPQ, may be localized to the nuclear compartment.[46] To test this theory, *SFPQ-ABL1*, *BCR-ABL1* and MSCV (control) were first overexpressed in HEK293T cells, and the localization of the ABL1 fusions was assessed by immunofluorescence. In this model, SFPQ-ABL1 was exclusively localized to the nucleus, unlike BCR-ABL1, which was predominantly localized to the cytoplasm (supplemental Figure 7). To confirm these findings in the context of B cells, we next analyzed Ba/F3 and wild-type pre–B cells transformed with BCR-ABL1 or SFPQ-ABL1. These experiments confirmed that although BCR-ABL1 was

localized in the cytoplasm in aggregates (Ba/F3) (Figure 3A) or diffusely (wild-type pre–B cells) (Figure 3B), SFPQ-ABL1 was primarily localized to the nucleus.

The ABL1 breakpoints do not account for phenotypic differences between SFPQ-ABL1 and BCR-ABL1

To determine whether the SH2/SH3 domains contribute to functional differences between the ABL1 fusions, we generated an SFPQ-ABL1 construct incorporating the SH2/SH3 domain (SFPQ-ABL1 + SH2/SH3), and BCR-ABL1 without these domains (BCR-ABL1 − SH2/SH3) (supplemental Figure 8). Interestingly, addition or deletion of the SH2/SH3 domains had no effect on the capacity of these fusion proteins to block IL-3 withdrawal–induced cell death in Ba/F3 cells (Figure 4A). Furthermore, inclusion of the SH2/SH3 domain in the SFPQ-ABL1 fusion protein did not increase the proliferative capacity to that of *BCR-ABL1*–expressing cells (Figure 4B).

To interrogate in an unbiased manner how the phosphoprotein networks of SFPQ-ABL1 and BCR-ABL1 may be altered by the presence or absence of the SH2/SH3 domains, we performed label-free quantification of phosphopeptides using mass spectrometry. We quantified a total of 24 532 phosphopeptides with a serine(S):threonine(T):tyrosine(Y) phosphosite ratio of 41.8:8.6:1. Although *SFPQ-ABL1* and *BCR-ABL1* expression was strikingly associated with distinct phosphoproteomic profiles, the addition of the SH2/SH3 encoding domains to *SFPQ-ABL1* did not drastically alter the phosphoproteome (Figure 4C; supplemental Figure 9). Together, these results suggest that the signaling and phenotypic differences observed between SFPQ-ABL1 and BCR-ABL1 cannot be primarily attributed to the different ABL1 breakpoints.

SFPQ-ABL1 and BCR-ABL1 activate distinct signaling networks

We performed 2 complementary approaches to identify sites that were differentially phosphorylated between *SFPQ-ABL1*– and *BCR-ABL1*–expressing cells (supplemental Figure 10). DPE analysis identifies peptides that are differentially phosphorylated independent of all other peptides, whereas DPU analysis identifies peptides that are differentially phosphorylated within a protein. DPE identified 2201 peptides, including 61 tyrosine (pY) sites, that were differentially phosphorylated in *SFPQ-ABL1*– and *BCR-ABL1*–expressing cells (supplemental Tables 1-2). Of the top differentially phosphorylated sites between *BCR-ABL1*– and *SFPQ-ABL1*–expressing cells (by adjusted *P* value), increased phosphorylation of proteins involved in signal transduction and known BCR-ABL1 adaptor

Figure 4. SFPQ-ABL1 and BCR-ABL1 activate distinct signaling networks. (A) Viability analysis of Ba/F3 cells expressing MSCV (empty vector control), *BCR-ABL1*, *BCR-ABL1* − SH2/SH3, *SFPQ-ABL1*, or *SFPQ-ABL1* + SH2/SH3, after 48-hour IL-3 withdrawal. Viability was determined by propidium iodide (PI) exclusion, measured by flow cytometry (n = 3). (B) Proliferation analysis of Ba/F3 cells expressing *ABL1* fusions after 48-hour withdrawal. Proliferation was measured by luminescence relative to MSCV empty vector control, using the CellTiter-Glo 2.0 reagent (n = 3). (C) Multidimensional scaling plot of label-free quantification phosphoproteomics data. Data were normalized, and missing peptide values were imputed by using a method based on low-rank decomposition. Data were corrected via Surrogate Variable Analysis to remove unwanted variation. Samples are colored according to the key in the top left corner of the plot. (D) Heat map showing top differentially phosphorylated sites between *BCR-ABL1*– and *SFPQ-ABL1*–expressing cells in DPE analysis. Expression for 16 samples (z score; scaled log2-intensity), including 4 biological repeats for each cell line, MSCV, BCR-ABL1, SFPQ-ABL1, and SFPQ-ABL1 + SH2/SH3, is shown (colored according to key, n = 4). Gene names and phosphorylation sites (in parentheses) are given on the right side of the heat map. (E) Differentially expressed KEGG pathways between *SFPQ-ABL1*– and *BCR-ABL1*–expressing cells. Sime's adjustment was applied to peptide *P* values to obtain protein level *P* values. limma was used to test for enriched KEGG terms. (F) Barcode plot of KEGG cell cycle proteins identified in DPE analysis. (G) Venn diagram of cell cycle proteins identified in phosphoproteomics analysis. Proteins were determined as differentially expressed if Sime's adjusted *P* value was < .05. logFC, log fold change.
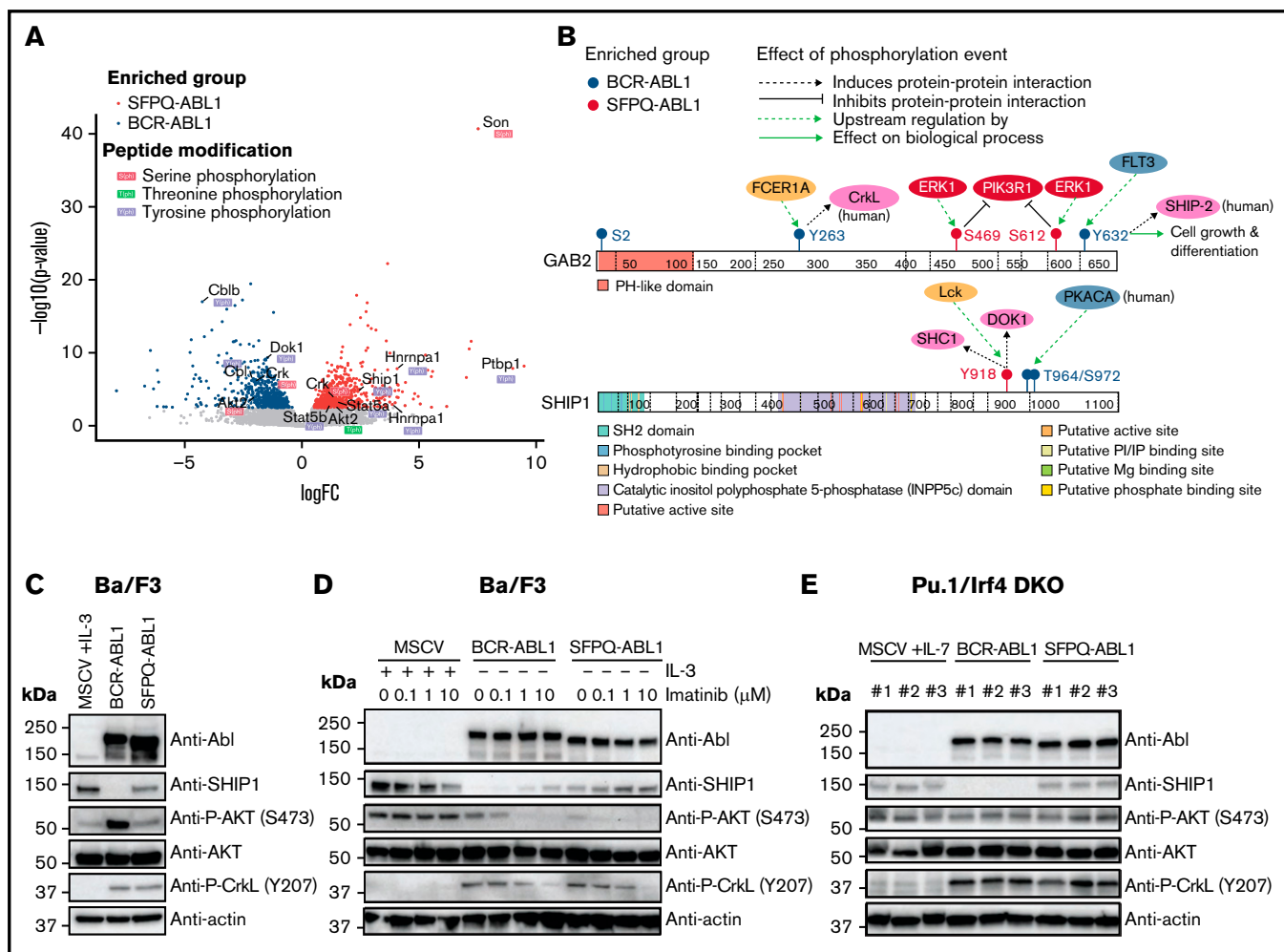
Figure 5. SPFQ-ABL1 and BCR-ABL1 differentially phosphorylate SHIP1 and GAB2. (A) Volcano plot of peptides identified in DPU analysis. Plots show log fold change (logFC) on the x-axis and $-\log10(P$ value) on the y-axis. Proteins/peptides of interest are labeled with gene name. Significantly enriched (P = .05) peptides and peptide modifications are colored according to the key in the top left of the plot. (B) Protein schematics of SHIP1 and GAB2 showing differential phosphorylation events identified in DPU analysis, produced by using ProteinPaint (Zhou et al *Nature Genetics*. 2016). Tyrosine phosphorylation events and resultant effects are coded according to the key in the top left corner. Functional domains are colored according to the key below each protein. (C) western blot analysis of SHIP1 and Phospho-AKT (P-AKT) expression in Ba/F3 cells expressing MSCV, *BCR-ABL1*, or *SFPQ-ABL1*. Pu.1/Irf4 DKO (representative western blot image is shown, n = 4). (D) western blot analysis of Ba/F3 cells treated with a dose titration (100 nM, 1 μM, and 10 μM) of imatinib for 6 hours (representative western blot image is shown, n = 3). (E) western blot analysis of SHIP1 and P-AKT in Pu.1/Irf4 DKO cells expressing MSCV, *BCR-ABL1*, or *SFPQ-ABL1*. Cell lines #1 to #3 represent 3 biologically independent cell lines.

proteins, including BCR-ABL1 Y177 interactors GAB2 and DOK1,[21,47] was observed in *BCR-ABL1*–expressing cells (Figure 4D). In *SFPQ-ABL1*–expressing cells, higher levels of phosphorylation in transcription factors and DNA/RNA binding proteins were observed. Notably higher phosphorylation levels of MLX, TPX2, SCMH1, PTBP1 (also known as hnRNP I), and DEPTOR (a negative regulator of mammalian target of rapamycin [mTOR]) was observed in *SFPQ-ABL1*–expressing and *SFPQ-ABL* + SH2/SH3*–expressing cells, suggesting that these proteins may be regulated by the SFPQ region of the fusion. Interestingly, reduced SHIP1 phosphorylation (encoded by *Inpp5d*) was exclusively observed in *BCR-ABL1*–expressing cells, compared with all other groups, consistent with previously published results.[48]

Pathway enrichment analysis was conducted on sites differentially phosphorylated between cells harboring *SFPQ-ABL1* or *BCR-*

ABL1 (Figure 4E). In total, 43 KEGG pathways showed evidence for differential regulation between the 2 fusions, the majority of which indicated increased signaling activity in *BCR-ABL1*–expressing cells. Specifically, NF-κB, MAPK, vascular endothelial growth factor, ErbB, and Ras signaling pathways, as well as the chronic myeloid leukemia pathway (specific for BCR-ABL1), were enriched in proteins with increased phosphorylation levels in *BCR-ABL1*–expressing cells (Figure 4E; supplemental Table 3). Enrichment for 7 KEGG pathways, including DNA replication, cell cycle, and spliceosome, were identified in *SFPQ-ABL1*–expressing cells. Enrichment of predominately nuclear pathways in *SFPQ-ABL1*–expressing cells is consistent with the localization of the fusion.

To assess the potential functional impact of increased phosphorylation of spliceosome proteins in *SFPQ-ABL1*–expressing cells, a comprehensive analysis of RNA-seq data was performed to
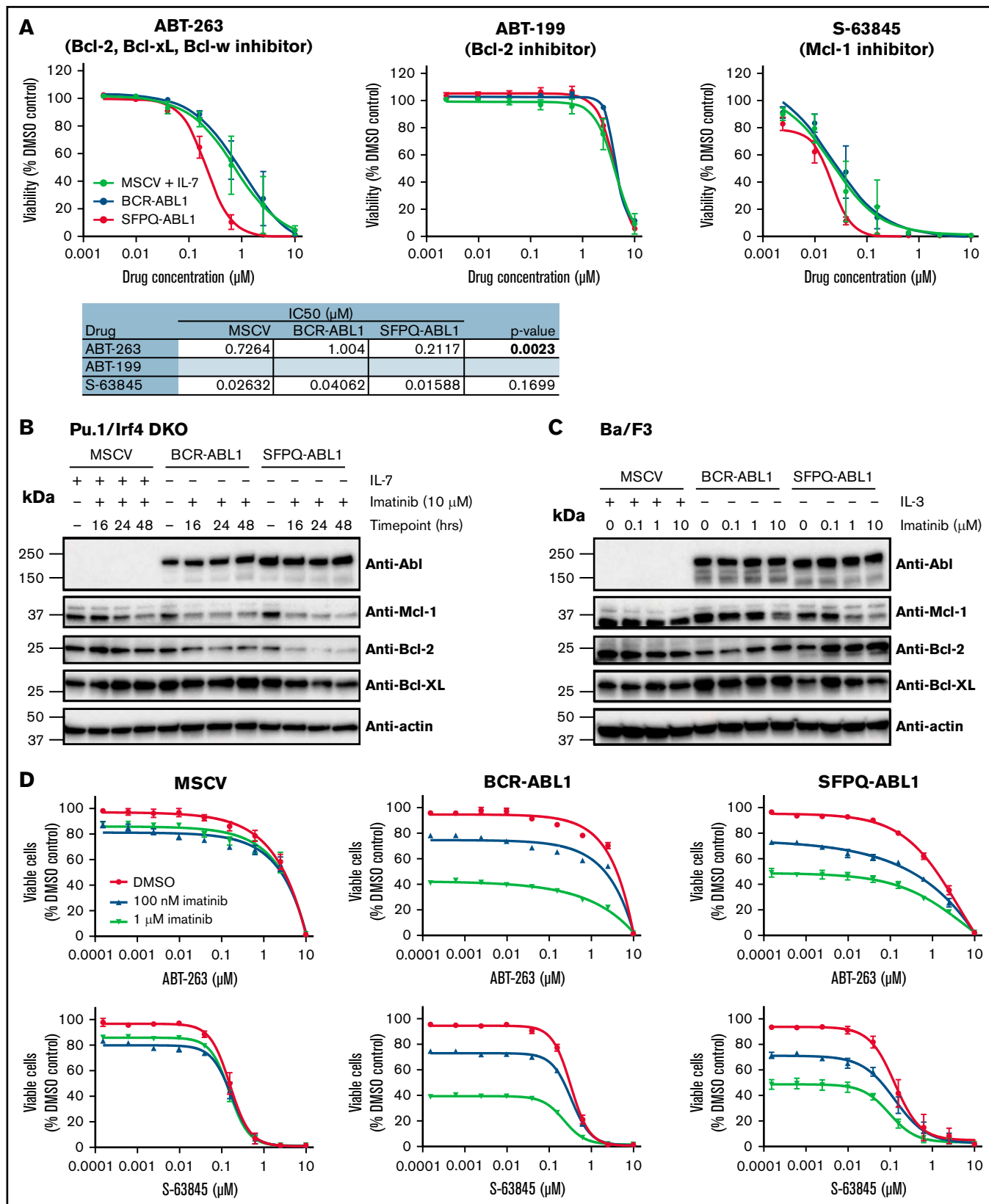
Figure 6. *SFPQ-ABL1*–expressing cells are sensitive to BH3 mimetics. (A) Viability analysis of Pu.1/Irf4 DKO cells expressing MSCV, *BCR-ABL1*, or *SFPQ-ABL1* treated with a dose titration of navitoclax, venetoclax, or S63845. MSCV control cells were treated in the presence of IL-7. Data are normalized to vehicle control (0.001% dimethyl sulfoxide [DMSO]; not shown on graphs), and nonlinear regression analysis was performed to fit dose–response curves and determine 50% inhibitory concentration

identify differential gene splicing between *SFPQ-ABL1–* and *BCR-ABL1–*expressing Ba/F3 cells. Across all 3 methodologies used (as discussed in the Methods), we identified evidence of differential splicing in only 43 genes, including Abl1, Bcr, and Sfpq, suggesting there is little difference in splicing overall (supplemental Table 4). Of note, reduced expression of known SFPQ transcriptional targets[32] was observed in *SFPQ-ABL1–*expressing cells, suggesting that the enforced SFPQ-ABL1 expression may antagonize wild-type SFPQ function (supplemental Figure 11).

SFPQ-ABL1 and BCR-ABL1 differentially phosphorylate cell cycle proteins

The cell cycle pathway was the most upregulated pathway (*P* = .0158) in *SFPQ-ABL1–*expressing cells (Figure 4E). In total, phosphoproteomics identified 78 proteins involved in the KEGG cell cycle pathway (supplemental Table 5), 5 with increased phosphorylation in *BCR-ABL1–*expressing cells and 29 in *SFPQ-ABL1–*expressing cells (Figure 4F-G). Analysis of specific phosphorylated sites in cell cycle proteins distinguished 39 that were differentially phosphorylated between *BCR-ABL1–* and *SFPQ-ABL1–*expressing cells (supplemental Tables 6-7). We observed increased phosphorylation levels of proteins involved in G1/S phase regulation, including cyclin D2 (CCND2), Rb, and p21[CIP1] (encoded by *Cdkn1a*) in *BCR-ABL1–*expressing cells, and proteins involved in G2/M phase regulation and DNA damage response in *SFPQ-ABL1–*expressing cells. Of particular interest in *SFPQ-ABL1–*expressing cells was increased phosphorylation of PLK1 pT210, a known activation residue,[49] and WEE1 pS139, predicted to mediate degradation of the protein and which could render cells sensitive to drugs targeting other checkpoint kinases.[50] To assess this, we treated Ba/F3 cells expressing either *BCR-ABL1* or *SFPQ-ABL1* with PLK1 inhibitors: BI2536 and BI6727 (volasertib), prexasertib (checkpoint kinase 1 [CHEK1] inhibitor), talazoparib (poly [ADP-ribose] polymerase [PARP] inhibitor), and berzosertib (ataxia telangiectasia and Rad3-related [ATX1] inhibitor). Interestingly, both ABL1 fusion–expressing lines tended to be more sensitive to the PARP inhibitor talazoparib, compared with the empty vector control, suggesting that ABL1 fusions may dysregulate DNA damage repair pathways.[51] However, there was no difference in response between cells expressing *SFPQ-ABL1* or *BCR-ABL1* to any of the inhibitors tested (supplemental Figure 12). These results suggest that although SFPQ-ABL1 differentially activates cell cycle and DNA damage response proteins compared with BCR-ABL1, this action does not result in differential sensitivity to drugs that target these pathways.

SPFQ-ABL1 and BCR-ABL1 differentially phosphorylate SHIP1 and GAB2

DPU analysis was used to identify specific phosphorylation sites regulated by SPFQ-ABL1 or BCR-ABL1 (Figure 5A; supplemental Table 8). In DPU analysis, a peptide is first compared between cell lines, in this case *BCR-ABL1–* and *SFPQ-ABL1–*expressing cells, and then ranked against all other peptides in the same protein to identify sites that are differentially phosphorylated within a protein. We focused on the 35 tyrosine sites that were differentially phosphorylated between *SFPQ-ABL1–* and *BCR-ABL1–*expressing cells (supplemental Table 9). Of these sites, 19 had a biological effect annotated in PhosphoSitePlus (supplemental Table 10). In general, increased phosphorylation of adaptor proteins involved in signal transduction pathways in *BCR-ABL1–*expressing and increased phosphorylation of transcription factors and spliceosome proteins in *SFPQ-ABL1–*expressing cells were observed. All 16 tyrosine sites enriched in *BCR-ABL1–*expressing cells have been previously identified in the phosphoproteome of p190 BCR-ABL1,[19,20] including GAB2 pY263 and pY632, which regulate interactions with CrkL (pY263) and SHP-2 (pY632), affecting cell growth and differentiation[52] (Figure 5B). Interestingly, GAB2 pS469 and pS612, which function in a negative feedback loop regulating phosphatidylinositol 3-kinase/protein kinase B (PI3K/AKT) signaling,[53] were more highly phosphorylated in *SFPQ-ABL1–*expressing cells.

Increased SHIP1 pY918 was observed in *SFPQ-ABL1–*expressing cells. Consistent with previous studies,[48] SHIP1 downregulation and increased AKT phosphorylation were observed in *BCR-ABL1–*expressing Ba/F3 cells. In contrast, Ba/F3 cells expressing *SFPQ-ABL1* maintain SHIP1 expression and AKT phosphorylation at levels similar to control cells (Figure 5C). Imatinib treatment of *BCR-ABL1–*expressing Ba/F3 cells, and to a lesser extent *SFPQ-ABL1–*expressing cells, increased the abundance of SHIP1 and reduced AKT phosphorylation (Figure 5D). In Pu.1/Irf4 DKO cells, we observed a similar pattern of SHIP1 expression in each of our 3 cell lines, although there was no difference in levels of Phospho-AKT (P-AKT) between these cell lines (Figure 5E). These data suggest that SFPQ-ABL1 may not activate AKT signaling to the same extent as BCR-ABL1.

Increased STAT5A pY694 and STAT5B pY699 were identified in *SFPQ-ABL1–*expressing cells in the phosphoproteomics analysis (supplemental Figure 13). However, in contrast to P-AKT, we did not detect a clear difference in the abundance of STAT5 phosphorylation (Y694) between *SFPQ-ABL1–* and *BCR-ABL1–*expressing cells, nor did we observe a difference in P-STAT5 expression after ruxolitinib treatment using western blotting (supplemental Figure 12B). Furthermore, we identified no specific STAT transcriptional activity associated with *SFPQ-ABL1* expression (supplemental Figure 13C). STAT5 activation is required for ABL1-fusion transformation, and these data suggest that as with BCR-ABL1, SFPQ-ABL1 promotes STAT5 phosphorylation, independent of JAK1/2.

SFPQ-ABL1–expressing cells are sensitive to BH3 mimetics

Both SFPQ-ABL1 and BCR-ABL1 block cytokine-withdrawal–induced cell death to drive transformation (Figures 1 and 2). To explore how SFPQ-ABL1 promotes cell survival, we first treated Pu.1/Irf4 DKO cells expressing *SFPQ-ABL1* or *BCR-ABL1* with BH3 mimetics with inhibitory activity against different pro-survival

---

Figure 6 (continued) (IC50) values (shown in table). Data are presented as mean ± standard error of the mean (n = 3). (B) western blot analysis of Pu.1/Irf4 DKO cells treated with 10 μM imatinib for 16, 24, or 48 hours. (C) western blot analysis of Ba/F3 cells treated with a dose titration of imatinib for 6 hours. (D) Viability analysis of Pu.1/Irf4 DKO cells expressing MSCV, BCR-ABL1, or SFPQ-ABL1 treated with a dose titration of ABT-263 or S63845 in the presence (100 nM or 1 μM) or absence (DMSO) of imatinib. MSCV control cells were treated in the presence of IL-7. Data are normalized to vehicle control (0.001% DMSO; not shown on graphs), and nonlinear regression analysis was performed to fit dose–response curves. Data are presented as mean ± standard error of the mean (n = 5).

proteins: ABT-263 (navitoclax), ABT-199 (venetoclax), and S-63845. All cell lines (including controls) were relatively resistant to ABT-199. Interestingly, cells expressing *SFPQ-ABL1* were more sensitive to ABT-263 ($P = .0023$) and S-63845, although not statistically significant, compared with *BCR-ABL1*–expressing cells (Figure 6A). We next harvested protein from imatinib-treated Ba/F3 and Pu.1/Irf4 DKO cells to analyze expression of pro-survival proteins. In Pu.1/Irf4 DKO cells, treated with 10 μM imatinib for 16, 24, and 48 hours, we observed a clear reduction in Mcl-1 and Bcl-2 expression over time in both fusion-expressing cell lines (Figure 6B). Bcl-xL was maintained in *BCR-ABL1*–expressing cells and to a lesser extent in *SFPQ-ABL1*–expressing cells when treated with imatinib. This relatively increased dependency on Bcl-xL for survival may explain the increased sensitivity of SFPQ-ABL1 to ABT-263. In Ba/F3 cells treated for 6 hours with imatinib, a dose-dependent reduction of Mcl-1 was observed, whereas Bcl-2 and Bcl-xL expression was maintained (Figure 6C). Lastly, we treated cells with a dose range of navitoclax and S-63845 as single agents or in combination with imatinib and showed that this combination had an additive effect on cell killing (Figure 6D; supplemental Figure 14).

Discussion

The current study presents the first functional analysis of the SFPQ-ABL1 fusion protein. Ph-like ALL patients harboring *ABL1* and *JAK2* rearrangements are predicted to respond to TKI therapy; however, these responses may be variable.[8-10] Functional characterization of rare ABL1 fusions provides important validating evidence for TKI therapy. Of the 3 reported *SFPQ-ABL1*^{+} ALL patients who have received TKI therapy (imatinib or dasatinib), all remained in remission for the period of study follow-up, suggesting that patients harboring this specific fusion respond well to TKIs.[12,25]

It is likely that acquisition of N-terminal dimerization domains of SFPQ facilitates oligomerization, resulting in transphosphorylation of the ABL1 kinase domain and signal transduction, as is the case for most ABL1 fusions.[17,54,55] In line with this, we show that SFPQ-ABL1 expression is sufficient to transform cytokine-dependent cells and drive constitutive expression of P-CrkL, which can be inhibited by ABL1-targeting TKIs. Although SFPQ-ABL1 lacks the SH2 and SH3 domains of ABL1, which normally function in the negative regulation of wild-type ABL1 kinase,[17] our data showed that restoration of these domains does not substantially alter the transforming capacity of SFPQ-ABL1. Instead, our experiments revealed that most of the key differences between SFPQ-ABL1 and BCR-ABL1 are the result of the fusion-specific N-terminal partner. Wild-type SFPQ functions to regulate pre-mRNA splicing,[31,56] nuclear retention of RNA,[29] and transcription,[32-34] and our global phosphoproteomics analysis suggests that SFPQ-ABL1 maintains some of these intermolecular interactions, which may be important for its function but do not result in discernible abnormalities in splicing.

SFPQ-ABL1 was as effective as BCR-ABL1 in blocking cytokine withdrawal–induced cell death but comparatively weak at promoting proliferation in the absence of cytokine. SFPQ-ABL1 is localized in the nuclear compartment, a feature it shares with NUP214-ABL1, which occurs almost exclusively in T-ALL.[57] NUP214-ABL1, localized to the nuclear pore complex, also has lower in vitro kinase activity, delayed transformation of Ba/F3 cells, and induction of longer latency leukemia in vivo, compared with BCR-ABL1.[22,23] Critically,

we found that nuclear localization does not, however, alter sensitivity to ABL1-targeting TKIs.

BCR-ABL1 activates PI3K/AKT signaling through multiple mechanisms, including GRB2/GAB2–mediated activation of PI3K[47] and downregulation of SHIP1.[58] Our data suggest that SFPQ-ABL1 does not exploit these mechanisms to activate PI3K/AKT signaling. Instead, *SFPQ-ABL1* expression promoted GAB2 pS469 and pS612, which negatively regulate PI3K/AKT signaling.[53] In addition, SHIP1 expression is not downregulated by SFPQ-ABL1, likely contributing to reduced PI3K/AKT pathway activation. Reduced PI3K/AKT signaling activation could, in turn, explain the reduced proliferative capacity of *SFPQ-ABL1*–expressing cells. In contrast, we show that as with BCR-ABL1,[59,60] SFPQ-ABL1 activates STAT5 in a JAK-independent manner. SFPQ-ABL1 is predominately localized in the nucleus, which raises the question of how this fusion phosphorylates predominately cytoplasmic unphosphorylated STAT5.[61] We speculate one of two possible explanations for the mechanism of phosphorylation: (1) SFPQ-ABL1 directly phosphorylates unphosphorylated STAT5 in the nucleus, as unphosphorylated STAT5A has been shown to be imported into the nucleus[62]; or (2) the more likely scenario, that there is sufficient SFPQ-ABL1 expressed in the cytoplasm to phosphorylate STAT5.

We also identified key differences in how SFPQ-ABL1 and BCR-ABL1 engage the cell cycle machinery, further highlighting the molecular distinctions between these seemingly similar kinase-activating fusions. *BCR-ABL1*–expressing cells were enriched for phosphorylation of proteins involved in G1/S phase regulation, whereas phosphorylation of proteins regulating G2/M phase and DNA damage response was a feature of *SFPQ-ABL1*–expressing cells. Enrichment of cell cycle proteins in *SFPQ-ABL1*–expressing cells is likely the result of its nuclear localization but did not confer a therapeutic sensitivity to PLK1 and DNA damage response inhibitors tested.

SFPQ-ABL1 and BCR-ABL1 both block cell death to transform cytokine-dependent cell lines. Dependencies on specific Bcl-2 family members for cell survival vary between driver fusions in B-ALL.[63] BCR-ABL1 requires Mcl-1 for leukemia initiation and maintenance, but this functional dependency can be overcome by overexpression of Bcl-2 or Bcl-xL.[64] These compensatory mechanisms that alter the balance of pro-survival Bcl-2 family proteins can potentially be exploited in combination therapies. Preclinical studies have shown that dual targeting of BCL-2 and MCL-1 may be effective in Ph+ and Ph-like ALL.[65] We show that, as with BCR-ABL1,[64] SFPQ-ABL1 maintains Mcl-1, as well as Bcl-xL, to promote cell survival, and this mediates sensitivity to ABT-263 and S-63845. We show that additional efficacy can be achieved when combining either of these agents with imatinib in *SFPQ-ABL1*–expressing cells.

This study highlights key functional and molecular differences between ABL1 fusions arising in B-ALL. The nuclear localization of SFPQ-ABL1 results in activation of signaling networks that are distinct from BCR-ABL1, but we show that the primary transformation event remains ABL1 kinase activation. We provide preclinical evidence that *SFPQ-ABL1*^{+} ALL patients will likely benefit from TKIs targeting ABL1.

Acknowledgments

Authorship

Contribution: L.M.B. performed biological experiments, curated phosphoproteomics and RNA-seq data, prepared figures and wrote the first draft of the manuscript; S.H.-Z. and H.H. performed bioinformatics analysis of phosphoproteomics and RNA-seq data; T.S. performed immunofluorescence analysis and biological experiments; J.J.S. prepared samples for phosphoproteomics and performed mass spectrometry; R.C.B. contributed to molecular cloning; H.J.K. prepared samples for RNA-seq; N.M.D. and B.S. assisted in bioinformatics analysis and interpretation; S.B., R.J., A.I.W., S.L.K., and A.O. provided intellectual input to the study and manuscript; P.G.E. and M.J.D. conceived and supervised the study; and L.M.B., T.S., and P.G.E. wrote the final version of the manuscript.

Conflict-of-interest disclosure: The authors declare no competing financial interests. P.G.E., R.C.B and M.J.D. are recipients of payments through the WEHI Distribution of Net Commercial Income program. The laboratory of R.W.J. receives research support from F. Hoffmann-La Roche Ltd., BMS, Astra Zeneca and MecRx. R.W.J. is a scientific consultant and shareholder in MecRx.

ORCID profiles: L.M.B., 0000-0002-4322-8203; S.H.-Z., 0000-0001-7513-6779; H.J.K., 0000-0002-0428-6195; S.B., 0000-0002-3012-9273; A.I.W., 0000-0001-5061-6995; A.O., 0000-0001-9788-5690; M.J.D., 0000-0003-4864-7033; P.G.E., 0000-0002-2976-8617.

Correspondence: Paul G. Ekert, Precision Medicine, Children's Cancer Institute, Lowy Cancer Centre, Sydney, NSW, Australia; e-mail: PEkert@ccia.org.au.

References

1. Roberts KG, Li Y, Payne-Turner D, et al. Targetable kinase-activating lesions in Ph-like acute lymphoblastic leukemia. *N Engl J Med.* 2014;371(11):1005-1015.

2. Mullighan CG, Su X, Zhang J, et al; Children's Oncology Group. Deletion of IKZF1 and prognosis in acute lymphoblastic leukemia. *N Engl J Med.* 2009;360(5):470-480.

3. Den Boer ML, van Slegtenhorst M, De Menezes RX, et al. A subtype of childhood acute lymphoblastic leukaemia with poor treatment outcome: a genome-wide classification study. *Lancet Oncol.* 2009;10(2):125-134.

4. Schultz KR, Bowman WP, Aledo A, et al. Improved early event-free survival with imatinib in Philadelphia chromosome-positive acute lymphoblastic leukemia: a Children's Oncology Group study. *J Clin Oncol.* 2009;27(31):5175-5181.

5. Schultz KR, Carroll A, Heerema NA, et al; Children's Oncology Group. Long-term follow-up of imatinib in pediatric Philadelphia chromosome-positive acute lymphoblastic leukemia: Children's Oncology Group study AALL0031. *Leukemia.* 2014;28(7):1467-1471.

6. Slayton WB, Schultz KR, Kairalla JA, et al. Dasatinib plus intensive chemotherapy in children, adolescents, and young adults with Philadelphia chromosome-positive acute lymphoblastic leukemia: results of Children's Oncology Group Trial AALL0622. *J Clin Oncol.* 2018;36(22):2306-2314.

7. Tanasi I, Ba I, Sirvent N, et al. Efficacy of tyrosine kinase inhibitors in Ph-like acute lymphoblastic leukemia harboring ABL-class rearrangements. *Blood.* 2019;134(16):1351-1355.

8. Tomita O, Iijima K, Ishibashi T, et al. Sensitivity of SNX2-ABL1 toward tyrosine kinase inhibitors distinct from that of BCR-ABL1. *Leuk Res.* 2014;38(3):361-370.

9. Ernst T, Score J, Deininger M, et al. Identification of FOXP1 and SNX2 as novel ABL1 fusion partners in acute lymphoblastic leukaemia. *Br J Haematol.* 2011;153(1):43-46.

10. Masuzawa A, Kiyotani C, Osumi T, et al. Poor responses to tyrosine kinase inhibitors in a child with precursor B-cell acute lymphoblastic leukemia with SNX2-ABL1 chimeric transcript. *Eur J Haematol.* 2014;92(3):263-267.

11. Ma X, Liu Y, Liu Y, et al. Pan-cancer genome and transcriptome analyses of 1,699 paediatric leukaemias and solid tumours. *Nature.* 2018;555(7696):371-376.

12. Biloglav A, Olsson-Arvidsson L, Theander J, Behrendtz M, Castor A, Johansson B. SFPQ-ABL1-positive B-cell precursor acute lymphoblastic leukemias. *Genes Chromosomes Cancer.* 2020;59(9):540-543.

13. Reshmi SC, Harvey RC, Roberts KG, et al. Targetable kinase gene fusions in high-risk B-ALL: a study from the Children's Oncology Group. *Blood.* 2017;129(25):3352-3361.

14. De Braekeleer E, Douet-Guilbert N, Guardiola P, et al. Acute lymphoblastic leukemia associated with RCSD1-ABL1 novel fusion gene has a distinct gene expression profile from BCR-ABL1 fusion. *Leukemia.* 2013;27(6):1422-1424.

15. De Braekeleer E, Douet-Guilbert N, Le Bris MJ, Berthou C, Morel F, De Braekeleer M. A new partner gene fused to ABL1 in a t(1;9)(q24;q34)-associated B-cell acute lymphoblastic leukemia. *Leukemia.* 2007;21(10):2220-2221.

16. Hidalgo-Curtis C, Chase A, Drachenberg M, et al. The t(1;9)(p34;q34) and t(8;12)(p11;q15) fuse pre-mRNA processing proteins SFPQ (PSF) and CPSF6 to ABL and FGFR1. *Genes Chromosomes Cancer.* 2008;47(5):379-385.

17. Hantschel O, Superti-Furga G. Regulation of the c-Abl and Bcr-Abl tyrosine kinases. *Nat Rev Mol Cell Biol.* 2004;5(1):33-44.

18. McWhirter JR, Galasso DL, Wang JY. A coiled-coil oligomerization domain of Bcr is essential for the transforming function of Bcr-Abl oncoproteins. *Mol Cell Biol.* 1993;13(12):7587-7595.

19. Cutler JA, Tahir R, Sreenivasamurthy SK, et al. Differential signaling through p190 and p210 BCR-ABL fusion proteins revealed by interactome and phosphoproteome analysis. *Leukemia.* 2017;31(7):1513-1524.

20. Reckel S, Hamelin R, Georgeon S, et al. Differential signaling networks of Bcr-Abl p210 and p190 kinases in leukemia cells defined by functional proteomics. *Leukemia.* 2017;31(7):1502-1512.

21. Puil L, Liu J, Gish G, et al. Bcr-Abl oncoproteins bind directly to activators of the Ras signaling pathway. *EMBO J.* 1994;13(4):764-773.

22. De Keersmaecker K, Rocnik JL, Bernad R, et al. Kinase activation and transformation by NUP214-ABL1 is dependent on the context of the nuclear pore. *Mol Cell.* 2008;31(1):134-142.

23. De Keersmaecker K, Versele M, Cools J, Superti-Furga G, Hantschel O. Intrinsic differences between the catalytic properties of the oncogenic NUP214-ABL1 and BCR-ABL1 fusion protein kinases. *Leukemia.* 2008;22(12):2208-2216.

24. Brown LM, Lonsdale A, Zhu A, et al. The application of RNA sequencing for the diagnosis and genomic classification of pediatric acute lymphoblastic leukemia [published correction appears in *Blood Adv.* 2020;4(7):1217]. *Blood Adv.* 2020;4(5):930-942.

25. Duhoux FP, Auger N, De Wilde S, et al. The t(1;9)(p34;q34) fusing ABL1 with SFPQ, a pre-mRNA processing gene, is recurrent in acute lymphoblastic leukemias. *Leuk Res.* 2011;35(7):e114-e117.

26. Sheng G, Zeng Z, Pan J, et al. t(1;9)(p34;q34)/SFPQ-ABL1 fusion in a patient with Ph-like common B-cell acute lymphoblastic leukemia. *Acta Haematol.* 2017;137(1):40-43.

27. Tran TH, Harris MH, Nguyen JV, et al. Prognostic impact of kinase-activating fusions and IKZF1 deletions in pediatric high-risk B-lineage acute lymphoblastic leukemia. *Blood Adv.* 2018;2(5):529-533.

28. Shav-Tal Y, Zipori D. PSF and p54(nrb)/NonO—multi-functional nuclear proteins. *FEBS Lett.* 2002;531(2):109-114.

29. Chen LL, Carmichael GG. Altered nuclear retention of mRNAs containing inverted repeats in human embryonic stem cells: functional role of a nuclear noncoding RNA. *Mol Cell.* 2009;35(4):467-478.

30. Fox AH, Lamond AI. Paraspeckles. *Cold Spring Harb Perspect Biol.* 2010;2(7):a000687.

31. Kim KK, Kim YC, Adelstein RS, Kawamoto S. Fox-3 and PSF interact to activate neural cell-specific alternative splicing. *Nucleic Acids Res.* 2011;39(8):3064-3078.

32. Roepcke S, Stahlberg S, Klein H, et al. A tandem sequence motif acts as a distance-dependent enhancer in a set of genes involved in translation by binding the proteins NonO and SFPQ. *BMC Genomics.* 2011;12(1):624.

33. Wang G, Cui Y, Zhang G, Garen A, Song X. Regulation of proto-oncogene transcription, cell proliferation, and tumorigenesis in mice by PSF protein and a VL30 noncoding RNA. *Proc Natl Acad Sci U S A.* 2009;106(39):16794-16798.

34. Imamura K, Imamachi N, Akizuki G, et al. Long noncoding RNA NEAT1-dependent SFPQ relocation from promoter region to paraspeckle mediates IL8 expression upon immune stimuli [published correction appears in *Mol Cell*. 2014;54(6):1055]. *Mol Cell.* 2014;53(3):393-406.

35. Uhrig S, Ellermann J, Walther T, et al. Accurate and efficient detection of gene fusions from RNA sequencing data. *Genome Res.* 2021;31(3):448-460.

36. Zhou X, Edmonson MN, Wilkinson MR, et al. Exploring genomic alteration in pediatric cancer using ProteinPaint. *Nat Genet.* 2016;48(1):4-6.

37. Ritchie ME, Phipson B, Wu D, et al. limma powers differential expression analyses for RNA-sequencing and microarray studies. *Nucleic Acids Res.* 2015;43(7):e47.

38. Hornbeck PV, Zhang B, Murray B, Kornhauser JM, Latham V, Skrzypek E. PhosphoSitePlus, 2014: mutations, PTMs and recalibrations. *Nucleic Acids Res.* 2015;43(database issue D1):D512-D520.

39. Hediyeh-zadeh S, Webb AI, Davis MJ. MSImpute: imputation of label-free mass spectrometry peptides by low-rank approximation. *bioRxiv.* 2020:2020.2008.2012.248963.

40. Phipson B, Lee S, Majewski IJ, Alexander WS, Smyth GK. Robust hyperparameter estimation protects against hypervariable genes and improves power to detect differential expression. *Ann Appl Stat.* 2016;10(2):946-963.

41. Perez-Riverol Y, Csordas A, Bai J, et al. The PRIDE database and related tools and resources in 2019: improving support for quantification data. *Nucleic Acids Res.* 2019;47(D1):D442-D450.

42. Zipfel PA, Zhang W, Quiroz M, Pendergast AM. Requirement for Abl kinases in T cell receptor signaling. *Curr Biol.* 2004;14(14):1222-1231.

43. de Jong R, ten Hoeve J, Heisterkamp N, Groffen J. Tyrosine 207 in CRKL is the BCR/ABL phosphorylation site. *Oncogene.* 1997;14(5):507-513.

44. Pang SH, Minnich M, Gangatirkar P, et al. PU.1 cooperates with IRF4 and IRF8 to suppress pre-B-cell leukemia. *Leukemia.* 2016;30(6): 1375-1387.

45. Mullighan CG, Miller CB, Radtke I, et al. BCR-ABL1 lymphoblastic leukaemia is characterized by the deletion of Ikaros. *Nature.* 2008;453(7191): 110-114.

46. Dye BT, Patton JG. An RNA recognition motif (RRM) is required for the localization of PTB-associated splicing factor (PSF) to subnuclear speckles. *Exp Cell Res.* 2001;263(1):131-144.

47. Sattler M, Mohi MG, Pride YB, et al. Critical role for Gab2 in transformation by BCR/ABL. *Cancer Cell.* 2002;1(5):479-492.

48. Sattler M, Verma S, Byrne CH, et al. BCR/ABL directly inhibits expression of SHIP, an SH2-containing polyinositol-5-phosphatase involved in the regulation of hematopoiesis. *Mol Cell Biol.* 1999;19(11):7473-7480.

49. Liu X, Zheng H, Li X, et al. Gain-of-function mutations of Ptpn11 (Shp2) cause aberrant mitosis and increase susceptibility to DNA damage-induced malignancies. *Proc Natl Acad Sci U S A.* 2016;113(4):984-989.

50. Ovejero S, Ayala P, Bueno A, Sacristán MP. Human Cdc14A regulates Wee1 stability by counteracting CDK-mediated phosphorylation. *Mol Biol Cell.* 2012;23(23):4515-4525.

51. Yi M, Dong B, Qin S, Chu Q, Wu K, Luo S. Advances and perspectives of PARP inhibitors. *Exp Hematol Oncol.* 2019;8(1):29.

52. Crouin C, Arnaud M, Gesbert F, Camonis J, Bertoglio J. A yeast two-hybrid study of human p97/Gab2 interactions with its SH2 domain-containing binding partners. *FEBS Lett.* 2001;495(3):148-153.

53. Zhang X, Lavoie G, Méant A, et al. Extracellular signal-regulated kinases 1 and 2 phosphorylate Gab2 to promote a negative-feedback loop that attenuates phosphoinositide 3-kinase/Akt signaling. *Mol Cell Biol.* 2017;37(7):e00357-16.

54. Wetzler M, Talpaz M, Van Etten RA, Hirsh-Ginsberg C, Beran M, Kurzrock R. Subcellular localization of Bcr, Abl, and Bcr-Abl proteins in normal and leukemic cells and correlation of expression with myeloid differentiation. *J Clin Invest.* 1993;92(4):1925-1939.

55. Cilloni D, Saglio G. Molecular pathways: BCR-ABL. *Clin Cancer Res.* 2012;18(4):930-937.

56. Ray P, Kar A, Fushimi K, Havlioglu N, Chen X, Wu JY. PSF suppresses tau exon 10 inclusion by interacting with a stem-loop structure downstream of exon 10. *J Mol Neurosci.* 2011;45(3):453-466.

57. Graux C, Cools J, Melotte C, et al. Fusion of NUP214 to ABL1 on amplified episomes in T-cell acute lymphoblastic leukemia. *Nat Genet.* 2004; 36(10):1084-1089.

58. Ruschmann J, Ho V, Antignano F, et al. Tyrosine phosphorylation of SHIP promotes its proteasomal degradation. *Exp Hematol.* 2010;38(5): 392-402, 402.e1.

59. Ilaria RL Jr, Van Etten RA. P210 and P190(BCR/ABL) induce the tyrosine phosphorylation and DNA binding activity of multiple specific STAT family members. *J Biol Chem.* 1996;271(49):31704-31710.

60. Hantschel O, Warsch W, Eckelhart E, et al. BCR-ABL uncouples canonical JAK2-STAT5 signaling in chronic myeloid leukemia. *Nat Chem Biol.* 2012;8(3):285-293.

61. Levy DE, Darnell JE Jr. Stats: transcriptional control and biological impact. *Nat Rev Mol Cell Biol.* 2002;3(9):651-662.

62. Iyer J, Reich NC. Constitutive nuclear import of latent and activated STAT5a by its coiled coil domain. *FASEB J.* 2008;22(2):391-400.

63. Brown LM, Hanna DT, Khaw SL, Ekert PG. Dysregulation of BCL-2 family proteins by leukaemia fusion genes. *J Biol Chem.* 2017;292(35): 14325-14333.

64. Koss B, Morrison J, Perciavalle RM, et al. Requirement for antiapoptotic MCL-1 in the survival of BCR-ABL B-lineage acute lymphoblastic leukemia. *Blood.* 2013;122(9):1587-1598.

65. Moujalled DM, Hanna DT, Hediyeh-Zadeh S, et al. Cotargeting BCL-2 and MCL-1 in high-risk B-ALL. *Blood Adv.* 2020;4(12):2762-2767.